Synthesis and Enhanced Lithium Storage Properties of Electrospun V2O5 Nanofibers in Full-Cell Assembly with a Spinel Li4Ti5O12 Anode

ARTICLE *in* ACS APPLIED MATERIALS & INTERFACES · APRIL 2013

Impact Factor: 6.72 · DOI: 10.1021/am400666n · Source: PubMed

3 AUTHORS, INCLUDING:

Yan Ling Cheah
Nanyang Technological University
23 PUBLICATIONS **1,364** CITATIONS
SEE PROFILE

Vanchiappan Aravindan
Nanyang Technological University
145 PUBLICATIONS **2,726** CITATIONS
SEE PROFILE

ACS APPLIED MATERIALS & INTERFACES

Research Article

www.acsami.org

Synthesis and Enhanced Lithium Storage Properties of Electrospun V_2O_5 Nanofibers in Full-Cell Assembly with a Spinel $Li_4Ti_5O_{12}$ Anode

Yan Ling Cheah,[†,‡] Vanchiappan Aravindan,*[,‡] and Srinivasan Madhavi*[,†]

[†]School of Materials Science and Engineering, Nanyang Technological University, Singapore 639798

[‡]Energy Research Institute @ NTU (ERI@N), Nanyang Technological University, Research Techno Plaza, 50 Nanyang Drive, Singapore 637553

Supporting Information

ABSTRACT: We have successfully demonstrated the reversible electrochemical Li-insertion properties of electrospun vanadium pentoxide nanofibers (VNF) in full-cell assembly with a $Li_4Ti_5O_{12}$ anode. Li-insertion in to VNF is restricted for the intercalation of 1 mol of Li by adjusting lower cutoff potential (2.5−4 V vs Li). The half-cell (Li/VNF) delivered a reversible capacity of ∼148 mA h g^{-1} with excellent cycleability and capacity retention of over 85% after 30 cycles. Full-cell assembly is conducted for such VNF cathodes after the electrochemical lithiation (LiV_2O_5) with spinel $Li_4Ti_5O_{12}$ anode under the optimized mass loadings. Full-cell ($LiV_2O_5/Li_4Ti_5O_{12}$) delivered an excellent cycleability irrespective of applied current densities with good reversible capacity of ∼119 mA h g^{-1} (at 20 mA g^{-1} current density). This work clearly demonstrates the possibility of using $LiV_2O_5/Li_4Ti_5O_{12}$ configuration for high power applications such as hybrid electric vehicles and electric vehicles in the near future.

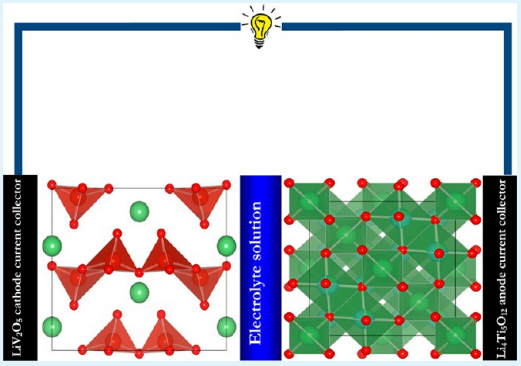

KEYWORDS: *Li-ion battery, cathode, vanadium pentoxide nanofibers, spinel $Li_4Ti_5O_{12}$ anode, full-cell, electrospinning*

INTRODUCTION

Lithium-ion batteries (LIBs) are attractive as one of the most ubiquitous electrochemical power sources in this era because of their widespread application in portable electronic devices such as laptops, cameras, personal digital assistants (PDAs), hand-held phones, etc.[1−7] The current research is directed towards employing such LIB power packs in hybrid electric vehicle (HEV) and electric vehicle (EV) applications.[8−10] The above-mentioned applications requires high energy density Li-ion power packs. Therefore a real platform for utilizing such power packs for HEV and EV applications lies in the development of high performance cathode materials.[8,11] Commercially available layered $LiCoO_2$ (theoretical capacity 274 mA h g^{-1}), spinel $LiMn_2O_4$ (theoretical capacity 148 mA h g^{-1}), and olivine $LiFePO_4$ (theoretical capacity 170 mA h g^{-1}) cathodes exhibited much less practical capacity than their theoretical limitations due to their own setbacks.[5,12] In addition, such cathodes endure a problem of high current operations, which prevents the possibility of using them in high power Li-ion power packs. Further, use of carbon coating or composites with carbonaceous materials results in reduction of volumetric capacity. Hence the search for alternate chemistries such as vanadium pentoxide (V_2O_5), olivines, silicates and NASICON-type materials, fluorophosphates, etc. is expected to fulfill the necessary demands for the development of high performance LIBs.[4,13] Among them, V_2O_5 is found to be promising because the arrangement of VO_5 octahedral units in layered structure enables reversible Li-insertion/extraction up to 3 mol which is feasible due to the multiple oxidation states of vanadium (V^{3+} to V^{5+}). Hence, achieving practical capacity over >300 mA h g^{-1} is possible for such V_2O_5 cathodes.[14−18] However, V_2O_5 cathodes undergo a structural change or irreversible transformation beyond 2 mol of Li-insertion which causes severe capacity fading upon cycling.[15] Therefore, several approaches like carbon coating and metallic doping are attempted with various morphologies to improve the battery performance.[19−21] On the other hand, improved cycleability can be achieved by limiting insertion to 1 mol of Li into the V_2O_5 matrix with theoretical capacity of 147 mA h g^{-1}. In this scenario, we made an attempt to develop one-dimensional vanadium pentoxide nanofibers (VNF) by a simple electrospinning technique. Generally, one-dimensional nanostructured cathode materials are favored to overcome the poor Li-ion kinetics observed in bulk systems by providing shorter Li-ion diffusion pathways. Also, electrospun VNF have a high aspect and surface-to-volume ratio which provides facile Li-diffusion via the enhanced electrode/electrolyte interface.[15,22] In our previous work, we demonstrated the enhanced battery performance of such one-dimensional (1 D) VNF by limiting various levels of Li-insertion.[15] Further improvements in the electrochemical performances of such VNF are also noted during Al^{3+} doping[23] and carbon coating by plasma enhanced chemical vapor

Received: February 21, 2013
Accepted: April 1, 2013
Published: April 1, 2013

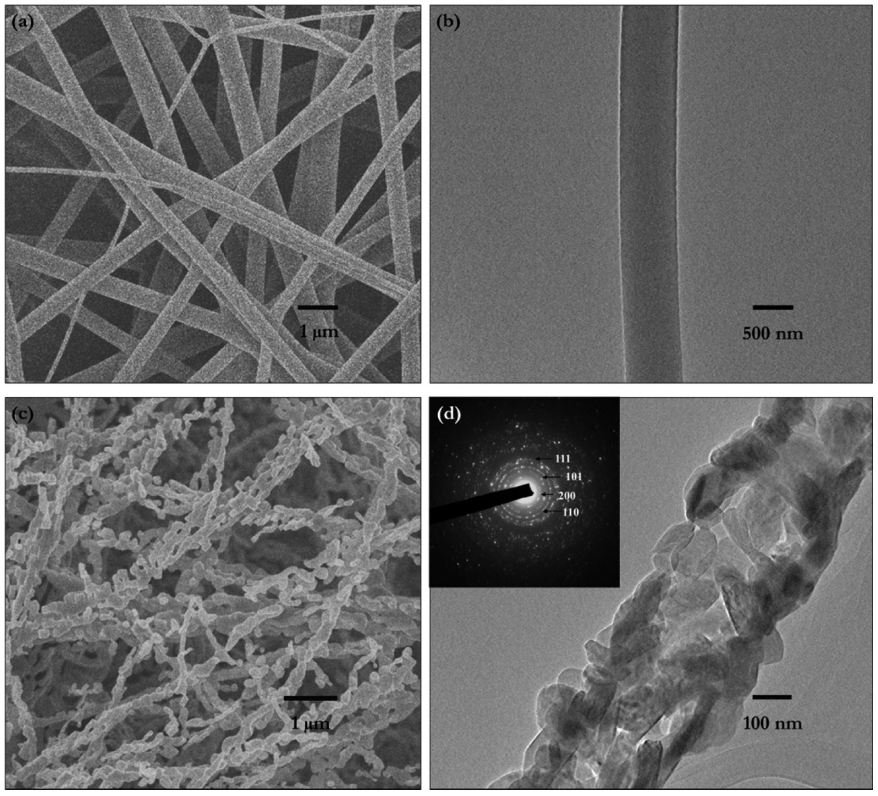

Figure 1. (a) Field emission scanning electron microscopy (FE-SEM) and (b) transmission electron microscopic (TEM) images of as-spun VNF; (c) FE-SEM and (d) TEM images of sintered VNF at 400 °C. (inset) SAED pattern.

deposition.[20] However, capacity fading still persists for the aforementioned approaches; in this line we attempted to restrict the Li-insertion to 1 mol by adjusting the cutoff potentials for the first time. Moreover, electrochemically lithiated VNF (LiV_2O_5) was used as a cathode along with the spinel $Li_4Ti_5O_{12}$ anode for the first time to construct the full-cell configuration. Detailed analysis about the performance of electrochemically lithiated VNF (hereafter abbreviated as Li-VNF) was studied with different current densities in full-cell assembly and presented in detail.

EXPERIMENTAL SECTION

One-dimensional VNF were synthesized via a simple and cost-effective electrospinning method and described in our previous reports.[20,15−27] In the typical synthesis procedure, vanadyl acetylacetonate ($VO(acac)_3$, 98%, Sigma-Aldrich), poly(vinylpyrrolidone) (PVP, M_w 360 000, Fluka), and acetic acid (Tedia Company Inc.) were mixed together in absolute ethanol (Fluka) and stirred continuously for 12 h. Then, the above solution was loaded into a syringe containing a stainless steel needle. Direct current (DC) voltage of 10 kV was applied between the needle tip and the aluminum foil collector which were separated by a distance of 10 cm. The flow rate was fixed at 2 mL h^{-1}. The electrospun fibers were collected as a mat, formed by random orientation of as-spun VNF over the Al foil. Then the mat was sintered using an alumina crucible at 400 °C for 15 min with a heating and cooling rate of 2 °C min^{-1} to yield a single-phase VNF.

Morphological features of as-spun and sintered VNF were studied by both field emission scanning electron microscopy (FE-SEM, JEOL JSM-7600F) and transmission electron microscopy (TEM, JEOL 2100F). Powder X-ray diffraction (XRD) measurements were used to study the structural properties of sintered VNF using D8 Advance instrument equipped with Cu Kα radiation. Rietveld refinement was also conducted for the obtained reflections using Topas V3 software. All the electrochemical studies were performed in two-electrode CR 2016 coin-cell configuration. The test electrodes were formulated with active material (VNF), conductive additive (Super P Li carbon, Timcal), and teflonized acetylene black (TAB-2, Hohsen Corporation, Japan) in the weight ratio of 5:2:1, respectively, using ethanol as the solvent. The electrode was pressed on a 200 mm^2 stainless steel mesh which served as a current collector. The composite electrodes were subsequently dried at 60 °C overnight before conducting cell assembly in Ar filled glovebox (MBraun, Germany). Li-insertion properties of VNF were evaluated in half-cell configurations (vs Li). For the full-cell assembly, the electrochemically lithiated VNF (Li-VNF) phase was used as cathode and spinel $Li_4Ti_5O_{12}$ as anode under the optimized mass loadings. Test electrodes in both configurations were separated by Celgard 2400 separator and filled with 1 M $LiPF_6$ in ethylene carbonate (EC):dimethyl carbonate (DMC) (Selectipure LP30, Merck KGaA, Germany) as the electrolyte solution. Swagelok fittings were also used for the electrochemical lithiation in to VNF (LiV_2O_5), which was used as the cathode in full-cell assembly. The lithiated phase was obtained by discharging the VNF in half-cell configuration to 2.5 V vs Li galvanostatically. Galvanostatic cycling profiles were conducted in ambient temperature conditions using the battery testing system Neware. Cyclic voltammetry (CV) was recorded using Solartron 1470E potentiostat using a standard two-electrode configuration at a slow scan rate of 0.1 mV s^{-1}.

RESULTS AND DISCUSSION

Morphological features of the electrospun VNF were analyzed through FE-SEM and TEM and presented in Figure 1. From the FE-SEM image of as-spun VNF (Figure 1a), the presence of highly interconnected network fibers with variation in the fiber diameters are clearly observed. A fiber diameter of 500−800 nm is noted for as-spun PVP/$VO(acac)_3$ composite fibers with a deviation of 50 nm. Very smooth surface morphology is evidenced from the TEM picture for as-spun fibers (Figure 1b). The calcination of as-spun fibers at 400 °C leads to the

formation of highly porous and large aspect ratio (>50) ultralong nanofibers (Supporting Information Figure S1). Small reduction in the fiber diameter is noted after the sintering process, which is presumably due to the evaporation of PVP and acetyl groups. Slow degradation of as-spun fibers during the sintering process results in the retention of fibrous morphology, which is composed of V_2O_5 nanoparticles grown along the fiber direction with porous structure clearly observed from the TEM image (Figure 1c and d).[15] Furthermore, it can be observed that the V_2O_5 nanocrystals are randomly oriented with average crystallite size of ~100 nm. Both FE-SEM and TEM observations are in good agreement with each other and showing fiber diameters are in the range of ~500−800 nm. The observed porous morphology in VNF is beneficial for the facile Li-ion diffusion under high current operations.[15] The selected area electron diffraction (SAED) pattern of sintered VNF (Figure 1d inset) showed concentric rings, which could be indexed to the *hkl* planes of (202), (101), (110), and (111), respectively. The presence of such concentric rings indicates the polycrystalline structure with no preferential orientation.

Structural properties of electrospun VNF were analyzed by XRD and refined with Rietveld refinement using TOPAS software and presented in Figure 2. From Figure 2, powder

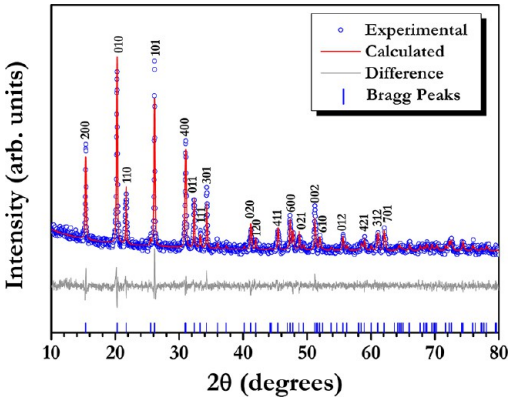

Figure 2. Rietveld refined powder X-ray diffraction pattern of VNF sintered at 400 °C.

XRD pattern clearly indicates the formation of phase pure structure without any impurity traces. Observed reflections for sintered VNF are indexed according to layered Shcherbinaite structure with $Pmn2_1$ space group. The lattice parameter values are calculated and found to be a = 11.518 (7) Å, b = 4.380 (3) Å, c = 3.567 (2) Å .The observed values are consistent with the literature values (JCPDS card no. 89-2482, a = 11.5202(3) Å, b = 4.3783(1) Å, and c = 3.5704(1) Å). Average crystallite size value is also calculated using Scherrer formulas during refinement and found to be ~98 (2) nm.

Li-insertion properties of electrospun VNF were evaluated by means of both galvanostatic and potentiostatic modes in half-cell configurations (Li/VNF). Generally, Li-insertion into V_2O_5 lattice results the transformation of V_2O_5 to $Li_xV_2O_5$ via different phases during multiple electron reaction. However, such a multiple Li-insertion process leads to the structural destruction/or irreversible phase transformation which causes severe capacity fading during cycling. In detail, when the test cell is discharged <2.0 V vs Li, V_2O_5 undergoes large distortion due to the accommodation of more than 2 mol of Li per formula unit ($Li_{2.2}V_2O_5$) and results in irreversible formation of the γ-$Li_xV_2O_5$ phase.[15,16] Hence an attempt has been made in the present case to restrict Li-insertion to 1 mol in the VNF (LiV_2O_5) lattice to retain the crystal structure with high reversibility, and this provides stable cycling performance (by keeping lower cutoff potential as 2.5 V vs Li). Generally, in the V_2O_5 matrix Li-ions are occupying the spaces between layers formed by VO_5 octahedral units in the V_2O_5 crystal structure.[16,24,28] According to the literature,[29−33] the intercalation of up to 1 mol of Li per V_2O_5 (by discharging to 2.5 V vs Li) leads to slight perturbation of the layered structure (δ-LiV_2O_5), thus maintaining good cycling behavior with minimal irreversible capacity. Restricted 1 mol Li-insertion to VNF is confirmed by XRD analysis and given in Suppporting Information Figure S2. Cyclic voltammograms (CV) were recorded for Li/VNF half-cell at slow scan rate of 0.1 mV s^{-1} between 2.5 and 4 V vs Li and shown in Figure 3. The test cells

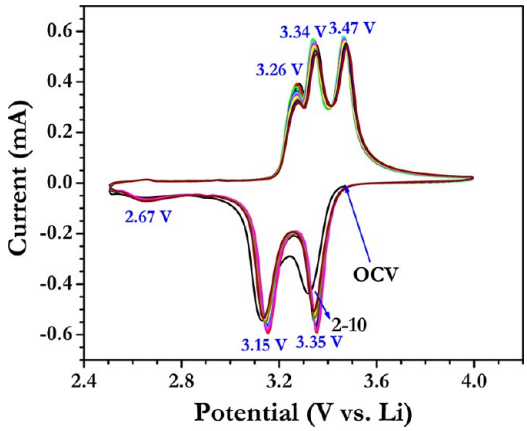

Figure 3. Cyclic voltammograms of VNF in half-cell assembly (Li/VNF) between 2.5 and 4.0 V vs Li at the slow scan rate of 0.1 mV s^{-1} at room temperature, in which metallic lithium acts as both counter and reference electrode.

exhibited very high open circuit voltage (OCV) ~3.4 V vs Li and subsequently discharged to 2.5 V vs Li for Li-insertion. From CV traces, it is apparent that VNF half-cells exhibited several oxidation/reduction peaks during both cathodic and anodic scan, which corresponds to reversible insertion and extraction processes of Li in the V_2O_5 lattice. In the first cathodic sweep, main reduction peaks are noted at ~3.32 and ~3.13 V vs Li, and also a small peak at ~2.6 V vs Li. On the other hand, three prominent oxidation peaks are observed at ~3.26, ~3.34, and ~3.47 V vs Li during a subsequent anodic sweep. The peak potential at ~3.32 V vs Li corresponds to the ε-$Li_{0.5}V_2O_5$ phase and peak potentials at ~3.13 and 2.60 V vs Li are ascribed to the δ-LiV_2O_5 phase formation[21] according to the following equilibria i and ii

$$V_2O_5 + 0.5Li^+ + 0.5e^- \leftrightarrow \varepsilon\text{-}Li_{0.5}V_2O_5 \quad \text{(i)}$$

$$\varepsilon\text{-}Li_{0.5}V_2O_5 + 0.5Li^+ + 0.5e^- \leftrightarrow \delta\text{-}LiV_2O_5 \quad \text{(ii)}$$

The overall reaction can be written as

$$V_2O_5 + Li^+ + e^- \leftrightarrow LiV_2O_5 \quad \text{(iii)}$$

CV studies are continued up to 10 cycles to ensure the reversibility and cycleability in the successive cycles which clearly evident that the reduction and oxidation peaks remain prominent. Interestingly, negligible shift in the reduction potential toward higher voltages are observed (~3.35 and ~3.15 V vs Li) upon subsequent cycling, whereas oxidation

potential remains unchanged. The small shift in the insertion potentials are very common for the case of insertion type materials which is presumably due to the crystal structure rearrangement/so-called formatting cycles. Prominent redox and overlapping peaks during subsequent cycles are attributed to the excellent reversibility of VNF during the Li-insertion/extraction process. Also, the current density of CV traces remains constant without significant reduction in area under the curve which indicates good cycling properties of such VNF in half-cell configuration.

Galvanostatic discharge−charge profiles of VNF in half-cell configurations (Li/VNF) were cycled between 2.5 and 4 V vs Li at a current density of 20 mA g^{-1} at room temperature and are shown in Figure 4. Specific capacity of ∼148 and ∼140 mA

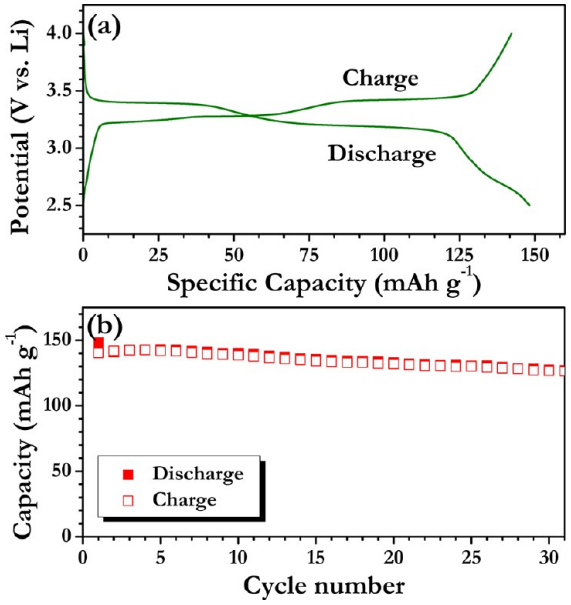

Figure 4. (a) Typical galvanostatic charge−discharge curves of VNF between 2.5 and 4.0 V vs Li in half-cell assembly (Li/VNF) and (b) Plot of specific capacity vs cycle number of VNF at current density of 20 mA g^{-1} at room temperature.

h g^{-1} is noted for the first discharge and charge, respectively. The observed discharge capacity value is the same as that of theoretical capacity for 1 mol Li-insertion whereas 0.95 mol Li only reversibly extracted from the lattice. In the discharge curve, long distinct plateaus are observed at ∼3.39 and ∼3.2 V followed by a kink-like plateau ∼2.7 V vs Li which is consistent with CV traces noted above. Instead of three peaks (observed in CV), only two distinct plateaus are obviously observed at ∼3.25 and ∼3.42 V, since peak potential difference (0.08 V) is found to be very small during the oxidation process. A plot of capacity vs cycle number for VNF in half-cell configuration at current density of 20 mA g^{-1} is presented in Figure 4b. Reversible capacity of ∼140 and ∼127 mA h g^{-1} is noted for the first and 30th cycle, respectively which corresponds to the capacity retention of ∼91% initial capacity. The observed cycling profile is one of the best values reported for V_2O_5 cathodes. Generally, V_2O_5 is believed to be a high capacity cathode for Li-ion batteries due to the multiple electron reaction (V^{5+} to V^{2+}). However irrespective of the morphology and synthesis procedures, V_2O_5 cathodes are experiencing severe capacity fade during cycling. So far, several approaches like carbon coating, composite with carbonaceous materials, shape controlled synthesis, etc., have been made to prevent the capacity fade. Nevertheless, such improvement in the capacity fading is still not sufficient to enable the application of V_2O_5 cathodes in practical Li-ion cells.[14] In the present case, compromising the capacity of V_2O_5 cathodes, Li-insertion is restricted to 1 mol, hence enhanced cycleability is achieved for such a one-dimensional VNF. Most of the commercially available cathodes such as $Li_{0.5}CoO_2$, $LiFePO_4$, $LiMn_2O_4$, and $Li(NiMnCo)_{1/3}O_2$ exhibit a practical capacity around ∼150 mA h g^{-1} with operating potential ranging from ∼3.4 to 4 V (vs Li). Nevertheless, operating potential of VNF is found ∼3.3 V vs Li, which is worth comparing with that of olivine $LiFePO_4$ (3.4 V vs Li) with a prominent plateau.

To demonstrate the performance of VNF in practical cells, a full-cell assembly is conducted with commercially available spinel $Li_4Ti_5O_{12}$ anode and cycled between 1 and 2.5 V at ambient temperature conditions. In the full-cell configuration, mass balance between the electrodes is very crucial to attain high performance Li-ion cells. Hence, a half-cell assembly is conducted for commercially available $Li_4Ti_5O_{12}$ ($Li/Li_4Ti_5O_{12}$) under the same current density between 1 and 3 V vs Li and given in Supporting Infomraiton Figure S3. On the basis of the electrochemical performance of VNF and $Li_4Ti_5O_{12}$ in half-cell configuration, mass loading between cathode and anode is fixed at a 1:0.82 ratio. Prior to full-cell assembly, VNF is electrochemically lithiated using Swagelok fittings by discharging to 2.5 V vs Li. CV studies are conducted for the full-cell assembly ($Li\text{-}VNF/Li_4Ti_5O_{12}$) at a slow scan rate of 0.1 mV s^{-1} and presented in Figure 5. In which CV traces of VNF and

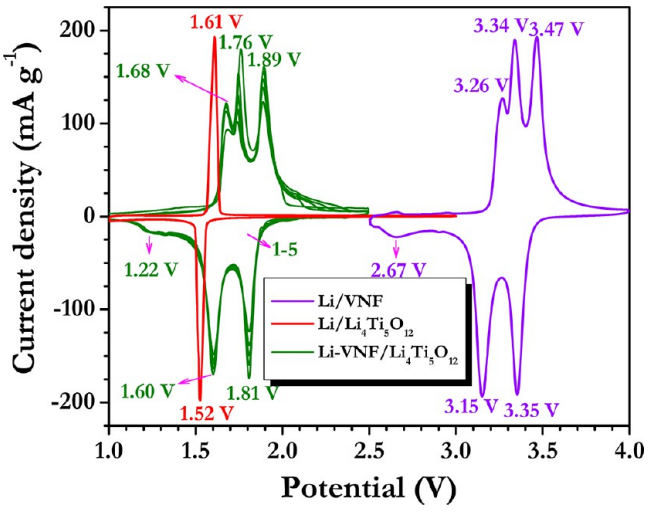

Figure 5. Cyclic voltammograms (CV) of electrochemically lithiated $VNF/Li_4Ti_5O_{12}$ full-cell configuration between 1.0 and 2.5 V at a scan rate of 0.1 mV s^{-1} at room temperature.

$Li_4Ti_5O_{12}$ in half-cell configurations are also given for the comparison. The oxidation peaks are observed at ∼1.68, 1.76, and 1.89 V whereas reduction peaks are noted at ∼1.81, 1.60, and 1.22 V in the $Li\text{-}VNF/Li_4Ti_5O_{12}$ cell. Oxidation (V^{4+} to V^{5+}) and reduction (V^{5+} to V^{4+}) peaks correspond to Li-extraction and reversible insertion, respectively. Further, the appearances of these peaks are consistent with those of VNF in half-cell configuration with shift in the peak potential due to the utilization of spinel $Li_4Ti_5O_{12}$. The minimal fade and negligible shift in current densities of the peaks are indicative of the good reversibility during cycling.

dx.doi.org/10.1021/am400666n | ACS Appl. Mater. Interfaces 2013, 5, 3475−3480

Galvanostatic cycling studies were conducted for Li-VNF/$Li_4Ti_5O_{12}$ cells at a constant current density of 20 mA g^{-1} and illustrated in Figure 6. The full cell delivered the capacities of

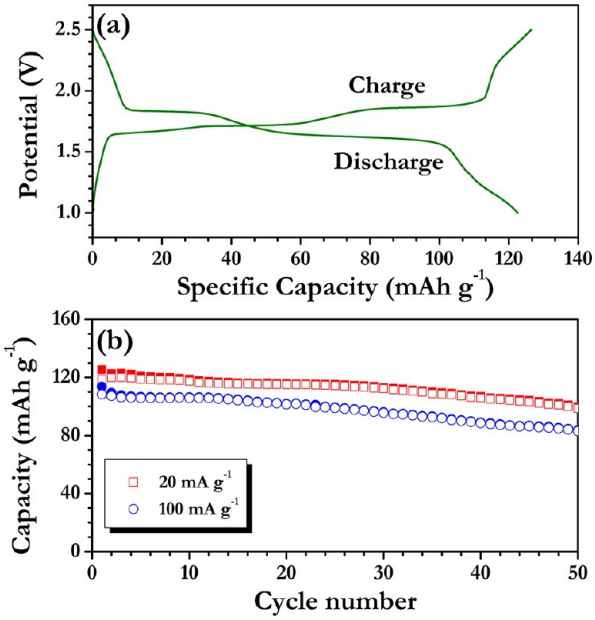

Figure 6. (a) Typical galvanostatic charge−discharge curves of electrochemically lithiated full-cell VNF/$Li_4Ti_5O_{12}$ between 1.0 and 2.5 V and (b) Plot of specific capacity vs cycle number at current densities of 20 and 100 mA g^{-1} at room temperature conditions. The filled and open symbols correspond to charge and discharge capacities, respectively.

~125 and 119 mA h g^{-1} in the first charge and discharge, respectively. Evident from Figure 6a are the two prominent plateaus during the charge (~1.70 and ~1.86 V) and discharge (~1.83 and 1.63 V) processes which is in good agreement with the CV traces and VNF in half-cell configuration as well. Galvanostatic cycling is extended to 50 cycles and presented in Figure 6b. Except for the initial few cycles, the coloumbic efficiency is found to be >98%. However, capacity fading is noted during cycling and ~84% of the initial capacity is retained with an operating potential of ~1.8 V. Capacity fade is mainly due to the poor compatibility of such vanadium based compounds toward linear carbonates (DMC) present in the electrolyte solution and intrinsic nature of the phase as well.[14,34] A similar kind of capacity fading is also noted for VNF in the half-cell assembly. In order to ensure our results, a duplicate cell has been made and tested at high current density of 100 mA g^{-1} and compared with low currents. After 50 galvanostatic cycles, the full cell retained ~77% of initial discharge capacity with coloumbic efficiency of over 98%. This enhanced performance of VNF is mainly attributed to the optimization of mass balance between the electrodes and synthesis of one-dimensional nanostructure prepared by electrospinning. Overall, restricted voltage range (2.5−4 V vs Li) applied to the electrochemical cycling of electrospun VNF enabled very high reversibility with operating potential of ~3.35 V vs Li with prominent plateaus. The limited Li-insertion leads to the negligible distortion between the layers consisting of VO_5 octahedra which provide very stable cycling performance.[15,28] The full-cell Li-VNF/$Li_4Ti_5O_{12}$ exhibits the energy density of ~215 W h kg^{-1} which is comparable with the $LiFePO_4$/$Li_4Ti_5O_{12}$ system.[7,35−37] Further studies such as carbon coating and usage of linear carbonate free electrolytes are in progress to improve the cycleability of VNF electrodes prepared by electrospinning.

CONCLUSION

Vanadium pentoxide nanofibers (VNF) were successfully synthesized via an electrospinning technique and studied by Rietveld refinement, FE-SEM, and TEM. Ultralong, high-aspect-ratio nanofibers with diameters 500−800 nm in a random network structure were observed and composed of nanoscopic V_2O_5 particulates. Restricted Li-insertion was conducted between 2.5 and 4 V vs Li to ensure the reversible insertion/extraction of 1 mol Li per formula unit. Highly reversible Li-insertion/extraction (0.95 mols of Li) was noted for VNF in the half-cell assembly. The full cell was constructed by optimized mass loadings of spinel $Li_4Ti_5O_{12}$ anode with operating potential of ~1.8 V. VNF-based electrodes experienced meager amount of capacity fade irrespective of the configurations (half-cell or full-cell) and delivered the energy density of ~215 W h kg^{-1} in full-cell assembly.

ASSOCIATED CONTENT

Supporting Information

TGA of as-spun VNF, XRD pattern of electrochemically lithiated VNF, and electrochemical performance of spinel $Li_4Ti_5O_{12}$ anode in half-cell configurations. This material is available free of charge via the Internet at http://pubs.acs.org.

AUTHOR INFORMATION

Corresponding Author

*E-mail: Madhavi@ntu.edu.sg (S.M.); aravind_van@yahoo.com (V.A.).

Notes

The authors declare no competing financial interest.

ACKNOWLEDGMENTS

This work was supported by funding from Competitive Research Programme (CRP) (Grant no. NRF-CRP4-2008-03) and Clean Energy Research Project (CERP) (Grant no. NRF-2009-EWT-CERP001-036). Authors also acknowledge Timcal for providing Super P Li Carbon black. The electron microscopy and XRD work were performed at the Facility for Analysis, Characterization, Testing and Simulation (FACTS) at Nanyang Technological University, Singapore.

REFERENCES

(1) Aravindan, V.; Gnanaraj, J.; Lee, Y.-S.; Madhavi, S. *J. Mater. Chem. A* **2013**, *1* (11), 3518−3539.
(2) Manthiram, A. *J. Phys. Chem. Lett.* **2011**, *2* (3), 176−184.
(3) Fletcher, S. *Bottled Lightning: Superbatteries, Electric Cars, and the New Lithium Economy*; Hill and Wang: New York, 2011.
(4) Goodenough, J. B.; Kim, Y. *Chem. Mater.* **2009**, *22* (3), 587−603.
(5) Reddy, C. V. S.; Jin, A.-P.; Han, X.; Zhu, Q.-Y.; Mai, L.-Q.; Chen, W. *Electrochem. Commun.* **2006**, *8*, 279−283.
(6) Scrosati, B.; Garche, J. *J. Power Sources* **2010**, *195* (9), 2419−2430.
(7) Hayner, C. M.; Zhao, X.; Kung, H. H. *Annu. Rev. Chem. Biomol. Eng.* **2012**, *3* (1), 445−471.
(8) Cairns, E. J.; Albertus, P. *Annu. Rev. Chem. Biomol. Eng.* **2010**, *1* (1), 299−320.
(9) Lee, K. T.; Cho, J. *Nano Today* **2011**, *6* (1), 28−41.
(10) Song, M.-K.; Park, S.; Alamgir, F. M.; Cho, J.; Liu, M. *Mater. Sci. Eng. R.* **2011**, *72* (11), 203−252.

(11) Park, O. K.; Cho, Y.; Lee, S.; Yoo, H.-C.; Song, H.-K.; Cho, J. *Energy Environ. Sci.* **2011**, *4* (5), 1621−1633.
(12) Fergus, J. W. *J. Power Sources* **2010**, *195* (4), 939−954.
(13) Gong, Z.; Yang, Y. *Energy Environ. Sci.* **2011**, *4* (9), 3223−3242.
(14) Chernova, N. A.; Roppolo, M.; Dillon, A. C.; Whittingham, M. S. *J. Mater. Chem.* **2009**, *19* (17), 2526−2552.
(15) Cheah, Y. L.; Gupta, N.; Pramana, S. S.; Aravindan, V.; Wee, G.; Srinivasan, M. *J. Power Sources* **2011**, *196* (15), 6465−6472.
(16) Cheah, Y. L.; Aravindan, V.; Madhavi, S. *J. Electrochem. Soc.* **2012**, *159* (3), A273−A280.
(17) Le, D. B.; Passerini, S.; Tipton, A. L.; Owens, B. B.; Smyrl, W. H. *J. Electrochem. Soc.* **1995**, L102−L103.
(18) Sakurai, Y.; Okada, S.; Yamaki, J.; Okada, T. *J. Power Sources* **1987**, *20*, 173−177.
(19) Sakunthala, A.; Reddy, M. V.; Selvasekarapandian, S.; Chowdari, B. V. R.; Selvin, P. C. *Energy Environ. Sci.* **2011**, *4* (5), 1712−1725.
(20) Cheah, Y. L.; von Hagen, R.; Aravindan, V.; Fiz, R.; Mathur, S.; Madhavi, S. *Nano Energy* **2013**, *2* (1), 57−64.
(21) Zhang, X.-F.; Wang, K.-X.; Wei, X.; Chen, J.-S. *Chem. Mater.* **2011**, *23* (24), 5290−5292.
(22) Cavaliere, S.; Subianto, S.; Savych, I.; Jones, D. J.; Roziere, J. *Energy Environ. Sci.* **2011**, *4* (12), 4761−4785.
(23) Cheah, Y. L.; Aravindan, V.; Madhavi, S. *ACS Appl. Mater. Interfaces* **2012**, *4* (6), 3270−3277.
(24) Mai, L.; Xu, L.; Han, C.; Yu, X.; Luo, Y.; Zhao, S.; Zhao, Y. *Nano Lett.* **2010**, *10*, 4750−4755.
(25) Wee, G.; Soh, H. Z.; Cheah, Y. L.; Mhaisalkar, S. G.; Srinivasan, M. *J. Mater. Chem.* **2010**, *20*, 6720−6725.
(26) Aravindan, V.; Cheah, Y. L.; Mak, W. F.; Wee, G.; Chowdari, B. V. R.; Madhavi, S. *ChemPlusChem* **2012**, *77* (7), 570−575.
(27) Mak, W. F.; Wee, G.; Aravindan, V.; Gupta, N.; Mhaisalkar, S. G.; Madhavi, S. *J. Electrochem. Soc.* **2012**, *159* (9), A1481−A1488.
(28) Pitchai, R.; Shivakumara, S.; Vasan, H. N.; Munichandraiah, N. *J. Phys. Chem. C* **2008**, *112*, 16700−16707.
(29) Cocciantelli, J. M.; Menetrier, M.; Delmas, C.; Doumerc, J. P.; Pouchard, M.; Broussely, M.; Labat, J. *Solid State Ionics* **1995**, *78*, 143−150.
(30) Delmas, C.; Cognac-Auradou, H.; Cocciantelli, J. M.; Menetrier, M.; Doumerc, J. P. *Solid State Ionics* **1994**, *69*, 257−264.
(31) Garcia, B.; Millet, M.; Pereira-Ramos, J. P.; Baffier, N.; Bloch, D. *J. Power Sources* **1999**, *81*, 670−674.
(32) Prouzet, E.; Moulin, C. C. d.; Villian, F.; Tranchant, A. *Faraday Trans.* **1996**, *92* (1), 103−109.
(33) Cocciantelli, J. M.; Doumerc, J. P.; Pouchard, M.; Broussely, M.; Labat, J. *J. Power Sources* **1991**, *34* (2), 103−111.
(34) Tanguy, F.; Gaubicher, J.; Soudan, P.; Bourgeon-Martin, N.; Mauchamp, V.; Guyomard, D. *Electrochem. Solid-State Lett.* **2007**, *10* (8), A184−A188.
(35) Thackeray, M. M.; Wolverton, C.; Isaacs, E. D. *Energy Environ. Sci.* **2012**, *5* (7), 7854−7863.
(36) Whittingham, M. S. *Proc. IEEE* **2012**, *100* (SPL CONTENT), 1518−1534.
(37) Besenhard, J. O.; Winter, M. *ChemPhysChem* **2002**, *3* (2), 155−159.